Journal of Neuropathology and Experimental Neurology
Copyright © 2003 by the American Association of Neuropathologists
Vol. 62, No. 1
January, 2003
pp. 88–103

PARP Expression Is Increased in Astrocytes but Decreased in Motor Neurons in the Spinal Cord of Sporadic ALS Patients

SEUNG H. KIM, MD, PHD, JENNY S. HENKEL, PHD, DAVID R. BEERS, PHD, IHSAN S. SENGUN, MD, ERICKA P. SIMPSON, MD, J. CLAY GOODMAN, MD, JOZSEF I. ENGELHARDT, MD, PHD, LÁSZLÓ SIKLÓS, PHD, AND STANLEY H. APPEL, MD

Abstract. The evidence for increased oxidative stress and DNA damage in amyotrophic lateral sclerosis (ALS) prompted studies to determine if the expression of poly(ADP-ribose) polymerase (PARP) is increased in ALS. Using Western analyses of postmortem tissue, we demonstrated that PARP-immunoreactivity (PARP-IR) was increased 3-fold in spinal cord tissues of sporadic ALS (sALS) patients compared with non-neurological disease controls. Despite the increased PARP-IR, PARP mRNA expression was not increased significantly. Immunohistochemical analyses revealed PARP-IR was increased in both white and gray matter of sALS spinal cord. While PARP-IR was predominantly seen in astrocytes, large motor neurons displayed reduced staining compared with controls. This result contrasts sharply to the staining of Alzheimer and MPTP-induced Parkinson diseased tissue, where poly(ADP-ribose) (PAR)-IR was seen mostly in neurons, with little astrocytic staining. PARP-IR was increased in the pellet fraction of sALS homogenates compared with control homogenates, representing potential PARP binding to chromatin or membranes and suggesting a possible mechanism of PARP stabilization. The present results demonstrate glial alterations in sALS spinal cord tissue and support the role of glial alterations in sALS pathogenesis. Additionally, these results demonstrate differences in sALS spinal motor neurons and astrocytes compared to brain neurons and astrocytes in Alzheimer disease and MPTP-induced Parkinson disease despite the presence of markers for oxidative stress in all 3 diseases.

Key Words: Amyotrophic lateral sclerosis (ALS); Astrocyte; Motor neuron; Poly(ADP-ribose) polymerase (PARP); Reverse transcriptase-polymerase chain reaction (RT-PCR); Western analysis.

INTRODUCTION

Amyotrophic lateral sclerosis (ALS) is a progressive fatal neurodegenerative disease involving both upper and lower motor neurons (1). While the molecular mechanisms that underlie motor neuron death in this disease are incompletely understood, oxidative stress is a prominent feature in sporadic ALS (sALS) (2–14). Markers of protein and lipid oxidation are elevated in postmortem tissue of sALS (2–5, 7, 8, 14). In addition, the level of 8-hydroxy-2′-deoxyguanosine (8OH2′dG), a marker of oxidative injury of DNA, increases with disease progression (7) and correlates with disease severity (11). These alterations were originally presumed to be largely confined to neurons. However, recent studies with spinal cords of sALS patients or ALS animal models demonstrate that markers of oxidative stress have been localized not only to motor neurons but also astrocytes, microglia, and macrophages (8, 14–18).

DNA damage by oxidation, alkylation, or ionizing radiation is associated with activation of poly(ADP-ribose) polymerase (PARP) (19–25). PARP is an abundant nuclear protein with a range of functions, including regulation of DNA repair, cell differentiation, and gene expression (26). When PARP is activated by DNA strand breaks, it subsequently transfers branched chains of ADP-ribose to a variety of nuclear proteins, including PARP itself (27). PARP can also be activated by inositol 1,4,5,-triphosphate-Ca^{++} mobilization without DNA damage (28). Ca^{++} promotes activation of PARP and Ca^{++} is an activating factor in PARP-mediated cell killing (24, 29). Although PARP facilitates DNA repair (30), excessive PARP activation can cause massive consumption of its substrate NAD^{+}, with resulting cell death due to energy depletion (19–21, 24, 27, 31–33).

Recently, the participation of PARP has been emphasized as a pathogenic mechanism in MPTP-induced Parkinson disease (34–37), Alzheimer disease (38), ischemic brain injury (39–44), and CNS trauma (45). Furthermore, PARP inhibitors have been proposed as potential therapies in neurodegenerative diseases in which oxidative stress is suspected to play an important pathogenic role (20, 23, 25, 34–37, 40–42, 46, 47). Despite the ample evidence for oxidative stress in the pathogenesis of ALS, the participation of PARP has not been carefully examined in this disorder.

From the Department of Neurology (SHK, JSH, DRB, ISS, EPS, SHA), and Department of Neurology and Pathology (JCG), Baylor College of Medicine, Houston, Texas; Department of Neurology (SHK), Hanyang University Hospital, Seoul, Korea; Department of Neurology (ISS), Dokuz Eylul University, Izmir, Turkey; Department of Neurology, University of Szeged (JIE), Szeged, Hungary; Department of Biophysics (LS), Biological Research Center, Szeged, Hungary.

Correspondence to: Stanley H. Appel, MD, Baylor College of Medicine, Department of Neurology, 6501 Fannin, Rm. NB302, Houston, TX 77030. E-mail: sappel@bcm.tmc.edu

This study was supported by the following grants: The Muscular Dystrophy Association, the Hamill Foundation (to SHA); National Scientific Research Fund of Hungary #OTKA T 034314 and #OTKA M 36252, Ministry of Health of Hungary #ETT T04/001/2000 (to LS); National Scientific Research Fund of Hungary #OTKA T 026239, Ministry of Health of Hungary #ETT T-05/28/2000 and #FKFP-0032/2000 (to JIE); Methodist grant #39655 (to DRB).

Downloaded from https://academic.oup.com/jnen/article/62/1/88/2917760 by Dokuz Eylul University Library (DEU) user on 02 September 2021

In this study, we investigated PARP immunoreactivity (PARP-IR) by Western analyses of postmortem spinal cord tissue from sALS patients compared with non-neurological disease controls. Semiquantitative reverse transcriptase-polymerase chain reaction (RT-PCR) was utilized to determine if the difference was due to an alteration in transcriptional regulation. Additionally, immunohistochemical analysis employing dual antibody labeling was used to determine the cell types expressing PARP-IR in sALS spinal cord.

MATERIALS AND METHODS

Postmortem Tissue of sALS and Control Patients

Spinal cord specimens were obtained at autopsy of sALS patients followed in the MDA/ALS Clinic at Baylor College of Medicine, Houston, TX (n = 7) or from the Brain Bank at the University Maryland, Baltimore, Maryland (n = 4). The clinical diagnosis was confirmed pathologically for all sALS patients. Postmortem samples from spinal cords of individuals with non-neurological diseases (n = 9) were used as controls. No pathological changes were present in the spinal cords of the control patients. The cause of death for patients in the sALS and control groups is shown in the Table. There was no significant difference between the average age of the patients in the sALS group (58.8 ± 12.7 yr) and the control group (57.9 ± 15.8 yr; $p > 0.4$; Table) or between the average time postmortem of the patients in the sALS group (13.4 h) and the control groups (13.7 h; Table). Sections from various levels of the spinal cords from each patient were either fixed in formaldehyde and embedded in paraffin, or were immediately frozen in liquid N_2 and stored at −80°C.

Western Blot Analysis

Approximately 300 μg samples were taken from the frozen spinal cord specimens without thawing. Whole spinal cord samples or dissected white and gray matter regions were homogenized on ice with a Wheatman homogenizer in a 20-mM HEPES buffer, pH 7.6, containing 200 mM KCl, 2 mM EGTA, 2 mM EDTA, 10 mM sodium molybdate, 50 mM sodium fluoride, 2 mM sodium pyrophosphate, 1 mM sodium vanadate, 0.1% NP-40, 10% glycerol, 4 mM benzamidine, 15 μg/ml aprotinin, 50 μM leupeptin, 1 μM pepstatin, and 1 mM phenylmethyl-sulfonyl fluoride. The homogenized samples were sonicated twice with Sonic 300 Dismembrator (Artek, Farmingdale, NY) for 20 s. Protein content was measured by the Bradford method (BioRad, Hercules, CA).

Two fractionation studies were performed. In the first fraction study, homogenized samples from each subject were divided in half; one half of the homogenized sample was used for PARP-IR and the second half was centrifuged for 30 min at 14,000 rpm (~15,000 *g*) at 4°C to separate the soluble and pellet fractions. The pellet fraction was dissolved in a buffer containing 0.5 M Tris, 4% SDS, 10% β-mercaptoethanol. Thus, 150 μg of total homogenate protein, 150 μg of soluble protein, and 150 μg of pellet protein were loaded on the gel. In the second fraction study, two 250-μg protein aliquots of the homogenized samples from each subject were used. One aliquot of the homogenized sample was used for PARP-IR and the other aliquot was centrifuged for 30 min at 14,000 rpm (~15,000 *g*) at 4°C to separate the soluble and pellet fractions. The pellet fractions were dissolved in a buffer containing 0.5 M Tris, 4% SDS, 10% β-mercaptoethanol. The entire soluble and pellet fractions and the 250-μg total homogenate aliquot were each loaded on the gel.

PARP and caspase 3 immunoreactivities were determined by immunoblot analyses. PARP was detected using the purified mouse anti-human PARP monoclonal antibodies 7D3–6 and C2–10 (Pharmingen, San Diego, CA). Goat polyclonal antibody, CPP32 (R&D systems, Minneapolis, MN) and rabbit polyclonal antibody, CM_1 (IDUN Pharmaceuticals, La Jolla, CA) were used to detect caspase-3. CPP32 was used to demonstrate both pro-caspase-3 and activated-caspase-3, while CM_1 (48, 49) detected only the activated form of caspase-3. Samples from sALS and control patients were subjected to 8% (for PARP), or to 4%–15% (for caspase-3) gradient sodium dodecyl sulfate polyacrylamide gel electrophoresis (SDS-PAGE) and transferred to nitrocellulose membranes.

The nitrocellulose membranes were blocked for 1 to 2 h at room temperature (RT) with 5% powdered milk in phosphate buffer saline containing 0.05% Tween-20 (PBST), then individually probed according to the manufacturer's recommendations for either PARP (1:1,000 for 7D3-6 and C2-10) or caspase-3 (1:1,000–2,000 for CPP32 and CM_1) overnight at 4°C. The membranes were processed using horseradish peroxidase-conjugated anti-mouse, anti-rabbit, or anti-goat secondary antibodies, and their signals detected using ECL chemiluminescence (Amersham Pharmacia, Piscataway, NJ). Sample loading and electroblotting in each experiment were evaluated by stripping the membranes (Reprobe, Geno Technology Inc., St. Louis, MO) and reprobing the membranes with an antibody to actin (A4700; Sigma, St. Louis, MO). The negatives were scanned with an HP ScanJet 6300C and densitometric analyses were conducted using Image-J software obtained from NIH image systems. The values are expressed as the mean ± SEM. Normalized PARP protein levels in the sALS and control groups were analyzed with the two-tailed Student *t*-test with unequal variances using Excel software. Differences were considered statistically significant with p values of 0.05 or less.

Measurement of PARP mRNA in Spinal Cord Samples

Total RNA was extracted (RNAeasy, Qiagen, Valencia, CA) from homogenized frozen whole spinal cord samples or from dissected white or gray matter regions. The RNA concentrations were determined spectrophotometrically (Beckman DU-64, Fullerton, CA). RT-PCR was performed using 10 ng of RNA according to the manufacturer's instructions (OneStep RT-PCR, Qiagen) using an Eppendorph Mastercycler (Westbury, NY). The PARP primers were designed using Primer 3 software (Baylor College of Medicine, Houston, TX) and were as follows: forward 5′-GCATCCTCTGAGTGGCCAGAA-3′ and reverse 5′-TCCGGGACTGACTGCAAAGAG-3′. The PCR protocol was 50°C for 30 min, 95°C for 15 min; (denatured at 95°C for 1 min, annealed at 60°C for 1 min, and extended at 72°C for 1 min 30 s) for 30 cycles; then 72°C for 5 min, and finally held at 4°C. The β-actin primers were 5′-GTGGGGCGCCCCAGGCACCA-3′ and 5′-CTCCTTAATGTCACGCACGATTTC-3′

Downloaded from https://academic.oup.com/jnen/article/62/1/88/2917760 by Dokuz Eylul University Library (DEU) user on 02 September 2021

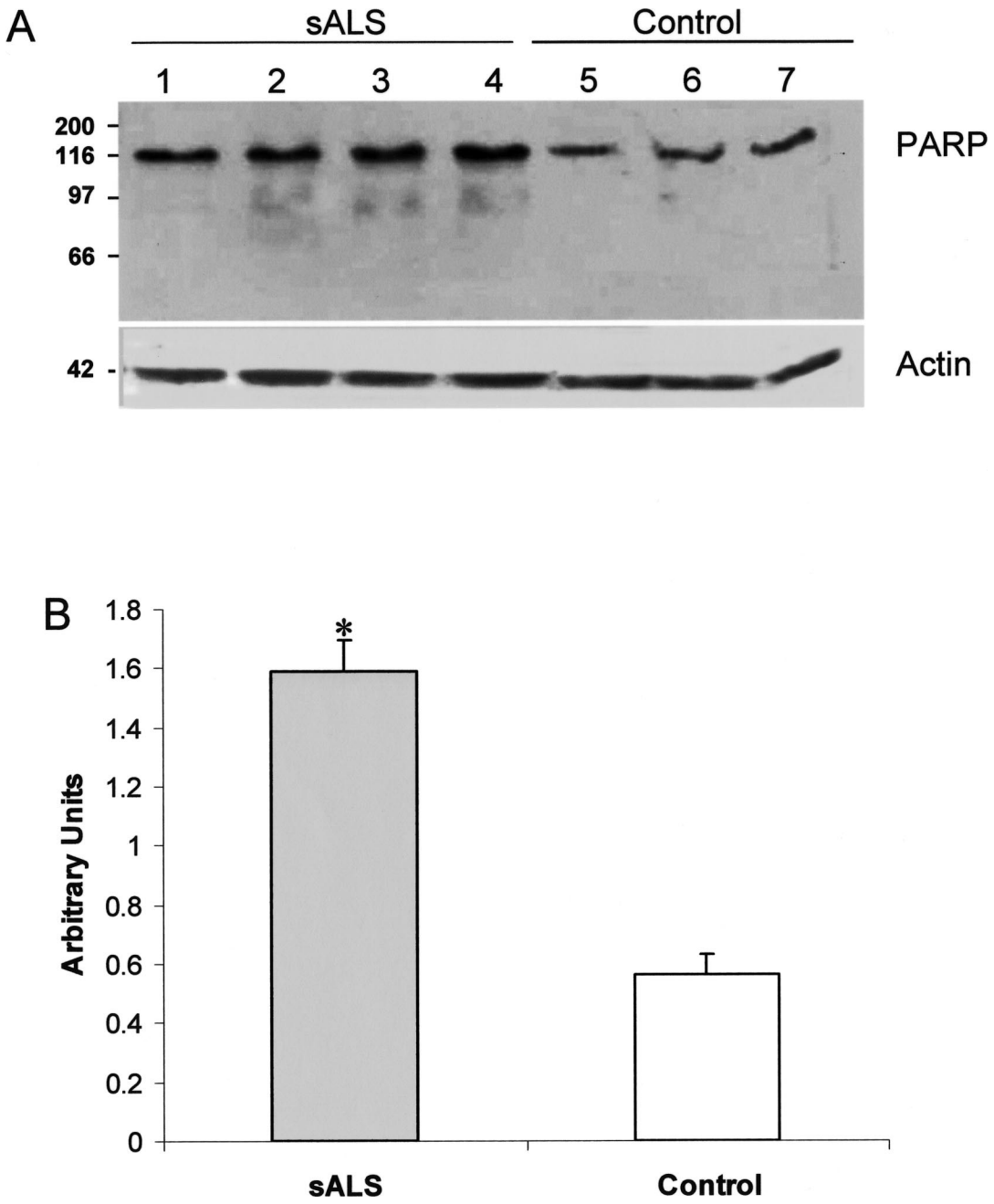

Fig. 1. PARP immunoreactivity in the spinal cord of sALS and control patients. **A:** A representative ECL immunoblot demonstrating increased PARP in spinal cord homogenates from sALS patients compared with controls (upper panel). Each well was loaded with 100 μg of total protein and blots were probed with anti PARP monoclonal antibody (7D3-6). The membranes were stripped and reprobed with anti-actin antibody as an internal control (lower panel). Positions of standard molecular weight markers in kilodaltons are indicated. **B:** Graphed quantitative data expressing PARP-IR levels normalized to actin from the sALS ($n = 8$) and control ($n = 5$) groups. PARP expression in the spinal cord of sALS patients was significantly larger than in controls (2.8-fold increase; $p < 0.0000024$). Each patient's data was represented by the average of 3 independent experiments. Data are reported as group means ± SEM.

as the forward and reverse primers, respectively (50). The β-actin PCR conditions were 50°C for 30 min, 95°C for 15 min; (denatured at 95°C for 1 min, annealed at 57°C for 1 min, and extended at 72°C for 1 min 30 s) for 38 cycles; then 72°C for 5 min, and finally held at 4°C. The RT-PCR products were resolved by 1.5% agarose/ethidium bromide gel electrophoresis and photographed under UV illumination. The negatives were scanned with an HP ScanJet 6300C and densitometric analyses were performed using the Image J software. Group means were analyzed with the two-tailed Student *t*-test with unequal variances using Excel software and plotted ± SEM; p values of 0.05 or less were considered statistically significant.

Downloaded from https://academic.oup.com/jnen/article/62/1/88/2917760 by Dokuz Eylul University Library (DEU) user on 02 September 2021

TABLE
Summary of Patients' Data

Case	Bank	Sex/age	Diagnosis	Cause of death	Postmortem	Analyses
ALS Patients						
1	B	M/40	sALS	respiratory failure	6 h	W, R
2	M	F/54	sALS	respiratory failure	3 h	W, R
3	M	F/66	sALS	respiratory failure	6 h	W
4	B	M/77	sALS	respiratory failure	15 h	W, R, I
5	M	M/69	sALS	respiratory failure	22 h	W, R
6	M	F/46	sALS	respiratory failure	3 h	W, R
7	B	M/53	sALS	respiratory failure	6 h	W, R I
8	B	F/71	sALS	respiratory failure	2.5 h	W, R, I
9	B	M/51	sALS	respiratory failure	12 h	I
10	B	M/73	sALS	respiratory failure	<48 h	I
11	B	M/47	sALS	respiratory failure	<24 h	I
Control Patients						
12	M	F/38	NND	drug poisoning	9 h	W, R
13	M	M/58	NND	MVA	18 h	W, R
14	B	M/39	NND	pulmonary embolism	17 h	W, R
15	M	F/66	NND	hypertension, sudden death	21 h	W, R
16	M	M/33	NND	asthma, sudden death	9 h	W, R
17	B	M/60	NND	cerebral infarct	3 h	I
18	B	F/64	NND	pneumonia	22 h	I
19	B	M/70	NND	myocardial infarction	19 h	I
20	B	M/76	NND	myocardial infarction	6 h	I

Postmortem = time postmortem prior to autopsy; h = hours; B = Brain Bank of Baylor College of Medicine, Houston; M = Brain Bank of University of Maryland, Baltimore; F = female; M = male; sALS = sporadic amyotrophic lateral sclerosis; NND = non-neurodegenerative disease; W = Western blot analysis; R = RT-PCR analysis; I = immunohistochemistry.

PARP Immunohistochemistry

Spinal cord samples were fixed in 10% neutral formaldehyde and embedded in paraffin. Five-μm-thick sections were cut from the blocks, deparaffinized, rehydrated, rinsed in tris-buffered saline (TBS, 50 mM; Sigma), and blocked for endogenous peroxidase activity (0.3% H_2O_2/methanol, 30 min). For antigen retrieval, sections were rinsed in TBS, placed in Na-citrate buffer (10 mM, pH 6.0; Sigma), and microwaved (3 × 5 min at 600 watts). To block nonspecific IgG binding, sections were cooled to RT, washed in TBS, and incubated for 20 min. in TBS containing 2% normal horse serum (Vector Laboratories, Burlingame, CA). Sections were incubated overnight at 4°C with a mouse monoclonal anti-human PARP antibody (Serotec, Raleigh, NC) according to the manufacturer's recommendations (1/100 dilution in TBS). Sections were rinsed in TBS and incubated in biotin-labeled horse-anti-mouse IgG (Vector Laboratories) (1/200 dilution in TBS, containing 2% normal horse serum) for 30 min at RT, rinsed in TBS, and further incubated in a biotin-avidin complex for 30 min (Vector Elite kit; Vector Laboratories), followed by washing in TBS. The immunoreaction was developed using an enhanced DAB substrate kit for 15 min (Pierce, Rockford, IL) and washed in distilled water. Sections were dehydrated, cleared in xylene, and coverslipped.

Immunostained sections were examined under a Zeiss Axioskop microscope (Karl Zeiss, Oberkochen, Germany) equipped with a DXC-970-MD CCD camera (Sony Corp., Japan) and a digital image analysis system (Optimas 6.2; Optimas Corp., Bothell, WA). Numbers of immunostained profiles (cell nuclei) in the white matter (lateral column) and gray matter (ventral horn) in sALS spinal cords versus controls were measured after setting the threshold for background staining. All imaging parameters (i.e. recording and illumination settings) were kept constant throughout the evaluation of the whole series. Eight fields were analyzed, 4 at the ventral horn and 4 at the lateral column. The average of the number of positive profiles was used to characterize the PARP-IR of the gray matter and the white matter of the spinal cord for each patient.

In addition, sections were double stained for glial fibrillary acidic protein (GFAP) and PARP to determine if astrocytes express increased PARP-IR. Following antigen retrieval and blocking nonspecific IgG binding sites, the sections were incubated with the PARP antibody (1:100 dilution; Serotec) and with 1:200 dilution of rabbit anti-cow GFAP antibody (DAKO A/S, Glostrup, Denmark) overnight at 4°C. Texas red labeled affinity purified goat anti-rabbit IgG and FITC conjugated horse anti-mouse affinity purified IgG (both from Vector Laboratories) were used as secondary antibodies.

RESULTS

PARP Levels in Spinal Cords of Patients with sALS

To determine if the level of PARP-IR was increased in sALS tissue, PARP protein from 8 sALS and 5 non-neurological disease control spinal cord tissue was assayed by Western analyses. Although 2 different antibodies were used initially to ensure we were detecting PARP; the majority of the analyses were performed with 7D3-6. Equivalent results were seen with both antibodies.

Downloaded from https://academic.oup.com/jnen/article/62/1/88/2917760 by Dokuz Eylul University Library (DEU) user on 02 September 2021

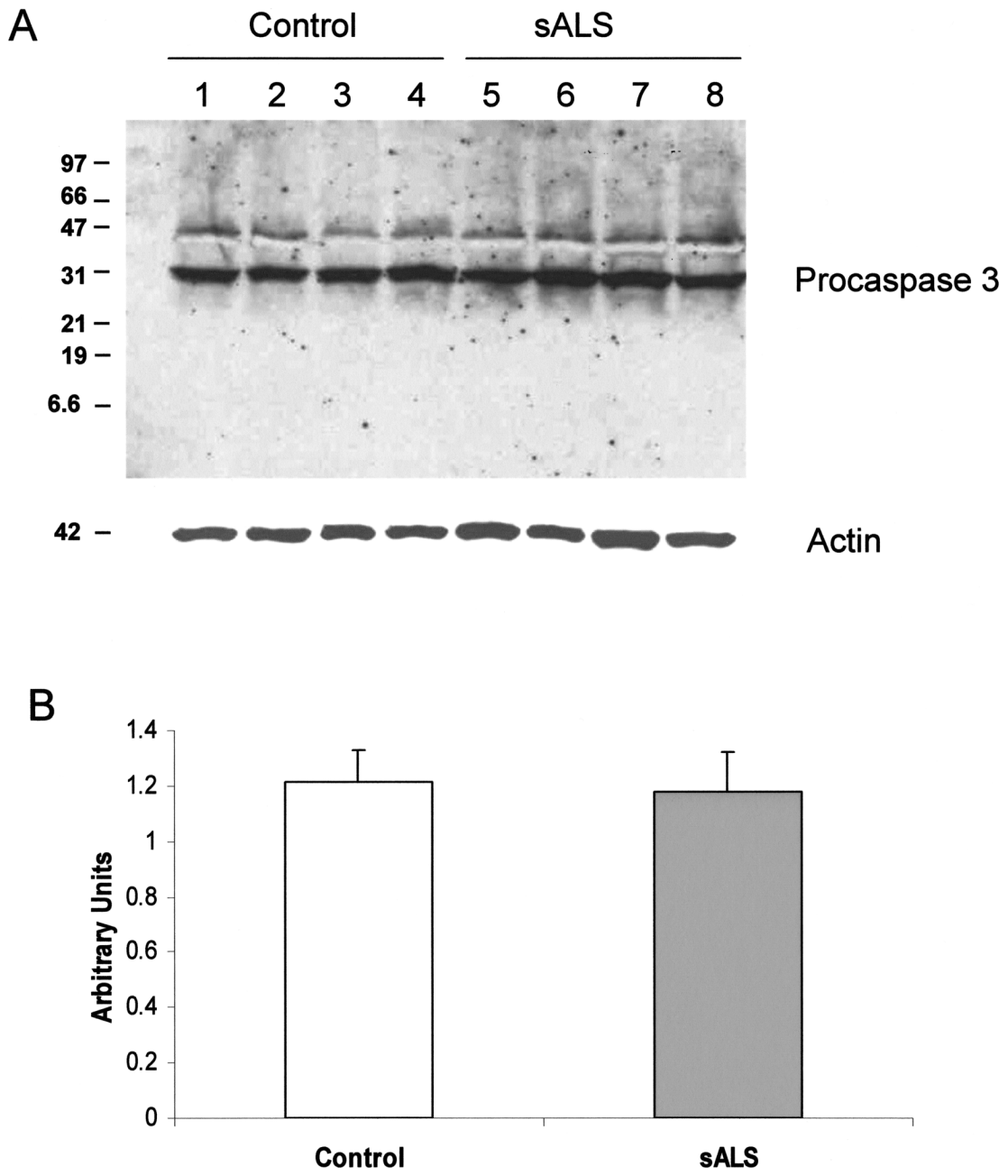

Fig. 2. Caspase-3-IR in the spinal cord from sALS. **A:** A representative ECL immunoblot assaying caspase-3 from spinal cord of sALS and controls patients (upper panel). Each well was loaded with 100 μg of total protein and blots were probed with the anti-caspase-3 polyclonal antibody CPP32. The membranes were stripped and reprobed with an anti-actin antibody as an internal control (lower panel). Molecular weights in kilodaltons are indicated. **B:** Graphed quantitative data for procaspase-3, after normalizing with actin data, demonstrates similar levels in the sALS and control groups. Data are reported as group means ± SEM.

Representative Western blots (Fig. 1A) demonstrate that PARP-IR was increased in the sALS spinal cord when compared with control. The quantified, normalized, and pooled data of the sALS and control patients (Fig. 1B) revealed that PARP-IR was 2.8-fold higher in sALS than controls ($p = 0.0000024$).

Caspase-3 Activation in the Spinal Cord

To examine whether pro- or activated caspase 3 expression was altered in sALS compared with control tissues, immunoblot analyses were performed with 4 sALS and 4 non-neurological disease control spinal cord

Downloaded from https://academic.oup.com/jnen/article/62/1/88/2917760 by Dokuz Eylul University Library (DEU) user on 02 September 2021

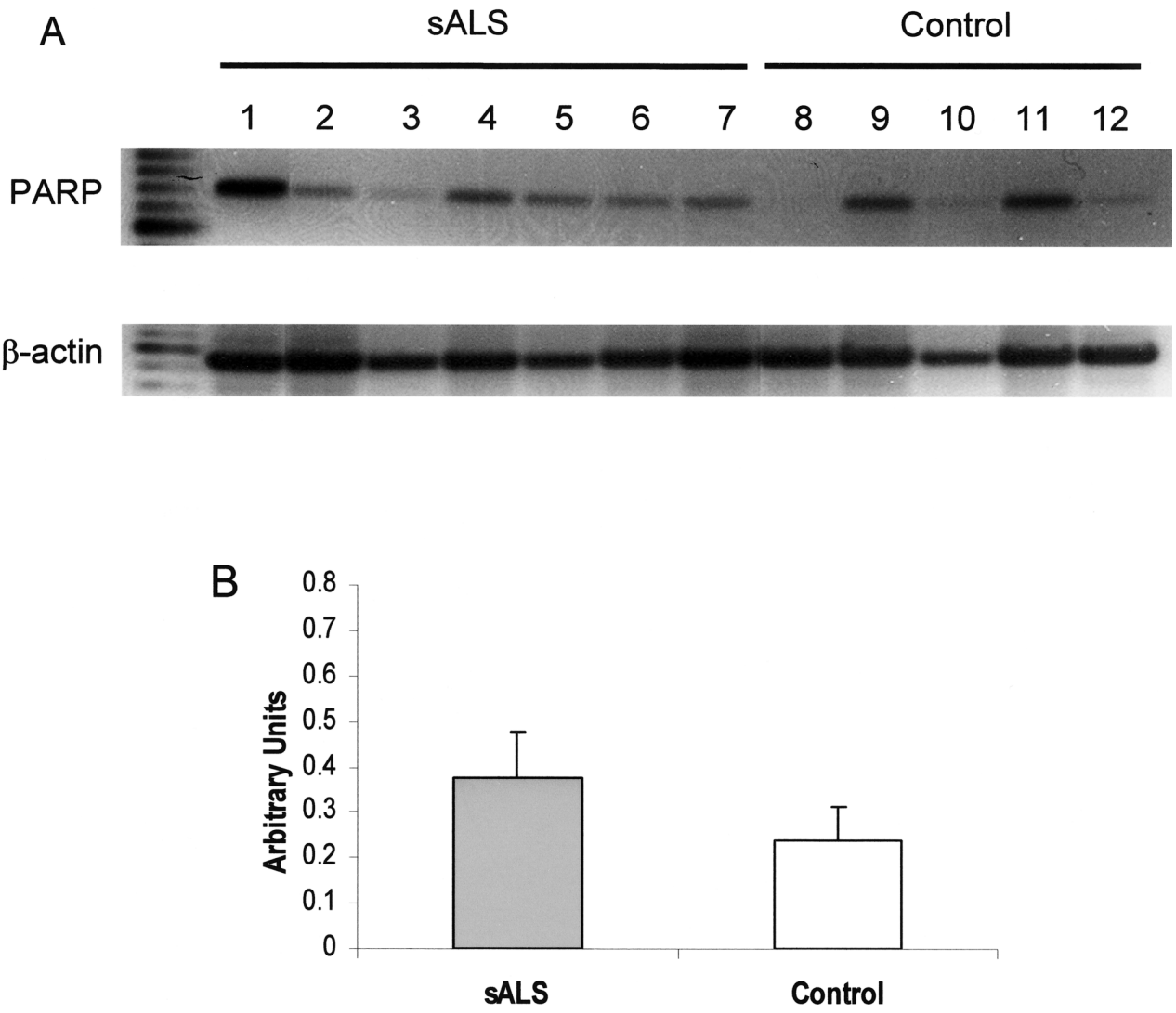

Fig. 3. mRNA for PARP in the spinal cord of sALS patients and controls. **A:** An agarose/ethidium bromide gel of PARP (upper panel) and β-actin (lower panel) RT-PCR products from sALS and control patients demonstrating comparable staining. **B:** Graphed quantitative data for PARP RT-PCR products, after normalizing to β-actin, demonstrate similar levels in the sALS and control groups. No significant differences could be demonstrated ($p = 0.27$). Data are reported as group means ± SEM.

samples using 2 different caspase-3 antibodies (CPP32 and CM_1). To control for recognition of activated caspase-3 by both antibodies, recombinant activated caspase-3 was used and could be recognized at ~17 kDa by both CPP32 and CM_1 (data not shown). Procaspase-3 immunoreactivity was readily detected in both sALS and control tissues; however, the immunoreactivity was similar in the 2 groups (Fig. 2A, B). No activated caspase-3 was detected in the spinal cord from sALS patients or controls using either antibody; however, the tissues we examined were harvested and frozen with an average delay of approximately 10 h postmortem.

Expression of PARP mRNA in the Spinal Cord

To ascertain whether the increase in PARP protein was due to an increase in PARP mRNA expression, spinal cords of sALS patients and controls were examined using semiquantitative RT-PCR. While the mRNA levels were examined in autopsy tissue, all of the levels were normalized with the internal control β-actin, which would control for mRNA integrity. Despite the increased levels of PARP protein in postmortem sALS tissue, no significant increase of the levels of PARP mRNA was detected ($p = 0.16$) (Fig. 3A, B). Thus the increased PARP protein detected in sALS tissue was not due to an increase in either PARP's transcription rate or mRNA stability.

Immunohistochemical Distribution of PARP-IR

To determine which cell types express the PARP-IR, we immunohistochemically examined spinal cord sections from sALS and control patients. PARP-IR was widespread in cells of control spinal cords, with higher

Downloaded from https://academic.oup.com/jnen/article/62/1/88/2917760 by Dokuz Eylul University Library (DEU) user on 02 September 2021

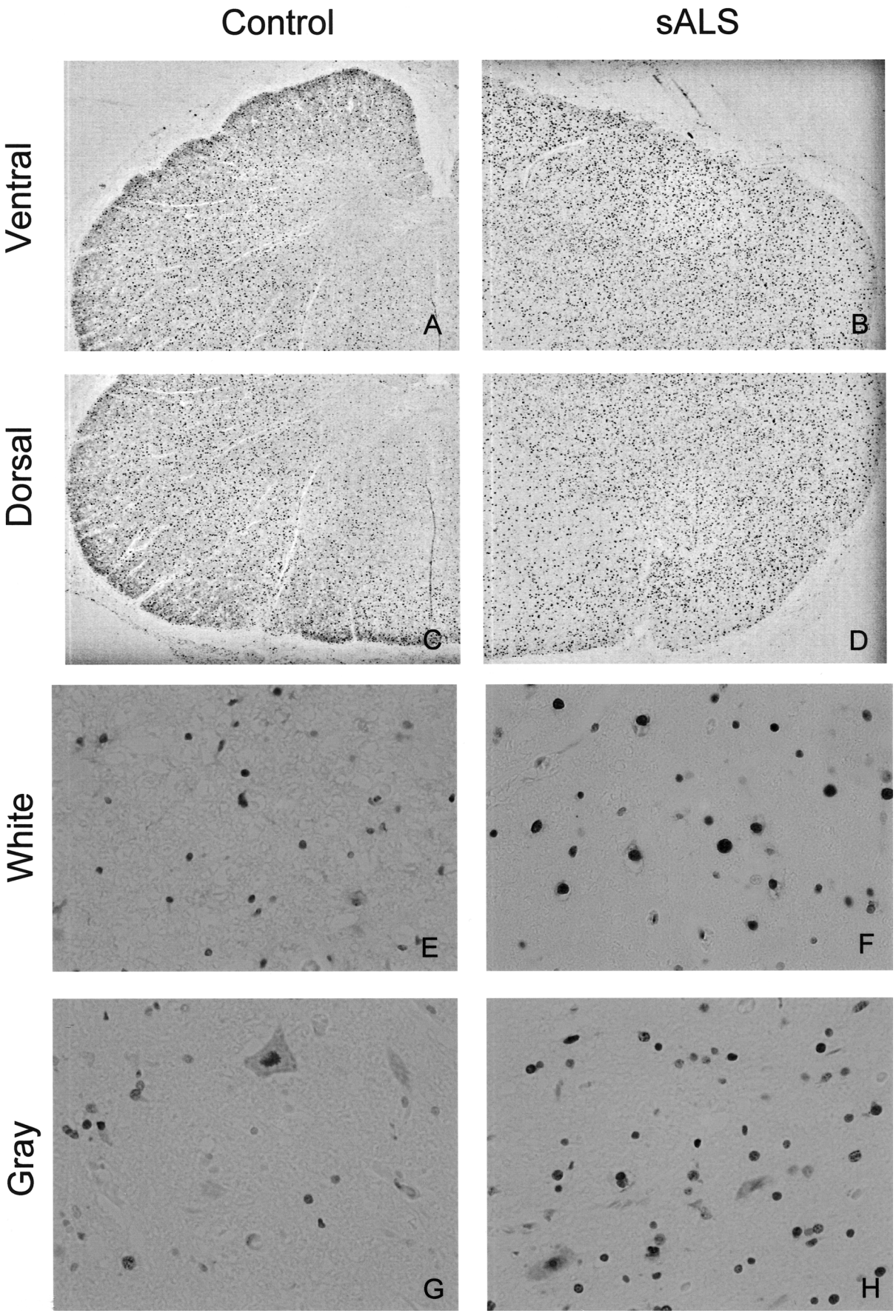

Downloaded from https://academic.oup.com/jnen/article/62/1/88/2917760 by Dokuz Eylul University Library (DEU) user on 02 September 2021

density of stained profiles in the white matter than in the gray matter. In sALS spinal cords, the number of PARP-immunoreactive cellular profiles was increased in both white and gray matter. However, the variability of this increase from patient-to-patient was larger in the gray matter than in the white matter. In both sALS and control sections, nuclei of both glial and neuronal cells were the primary structures stained (Fig. 4E–H). The PARP-IR was predominantly in cells with glial morphology, typically astrocytic morphology. Double immunostaining for PARP and for GFAP demonstrated that most of the PARP-immunoreactive cells in the white matter were astrocytes (Fig. 5B).

Quantitative analyses were performed to determine the number of stained profiles in tissue domains of equal size in the gray and white matter of sALS and control spinal cord sections. Increased PARP-IR was present in the white matter of sALS spinal cords compared with controls, predominantly in cells with glial morphology (Fig. 5C). Increased PARP-IR, also predominantly in cells with glial morphology, was present in the gray matter of sALS sections as well, but was far more variable (Fig. 5C). Proportionately larger increases were present in the gray matter (2.7×) than in the white matter (1.8×), but only the latter was statistically significant ($p < 0.016$).

PARP staining of motor neurons was examined in sALS and control spinal cord sections. Motor neurons were identified according to their size and position in the ventral horn. Those motor neurons with readily discernible nuclei were assessed for PARP immunostaining (Fig. 6A, B). Thirty-nine control neurons and 36 ALS neurons were counted. PARP-positive motor neurons were less frequently detected in sALS sections than in control sections. As a percentage of motor neurons counted, the control sections contained 75.5% ± 3.7% PARP-positive motor neurons, while sALS sections had 23.8% ± 11.0% PARP-positive motor neurons (Fig. 6C; $p < 0.0014$).

PARP Levels in Spinal Cords of Patients with sALS

Parallel Western and semiquantitative RT-PCR analyses were performed on sALS and control white and gray matter spinal cord specimens. PARP-IR was increased in the white matter of sALS spinal cord compared with control ($p = 0.04$), but not in the gray matter ($p = 0.53$) (Fig. 7A). Interestingly, PARP mRNA expression was not significantly increased in the white ($p = 0.32$) or the gray matter ($p = 0.62$) of sALS tissue compared with control tissue (Fig. 7B). Thus, the increase in PARP expression seen in the sALS tissue is not due to a significant increase in PARP transcription or mRNA stability, but is due to a net increased rate of translation, increased protein stability, and/or decreased protein degradation.

Distribution of PARP Expression in the Soluble and Pellet Fractions

To examine whether the increased PARP-IR in sALS might be related to altered distribution (and perhaps stabilization) of PARP protein, we compared levels of PARP-IR in whole spinal cord homogenate, soluble, and pellet fractions from sALS and control patients. We performed 2 fractionation studies. In the first study we examined equal amounts of protein from each fraction. Figure 8A shows an immunoblot evaluating 150 μg protein from the total homogenate (H) and 150 μg protein from each of the soluble (S) and pellet (P) fractions. PARP-IR in the sALS sample was dramatically increased in the pellet fraction and decreased in the soluble fraction when compared with the control sample. In the second fractionation study, we examined how PARP separated into soluble and pellet fractions from a specific amount of spinal cord homogenate. One 250-μg aliquot of homogenate was separated into soluble (S) and pellet (P) fractions and compared with an identical unseparated 250-μg aliquot. As shown in Figure 8B, a short 30-s exposure revealed increased PARP-IR in whole homogenate and pellet fractions in sALS compared with controls. A 10-min exposure further revealed PARP-IR was decreased in soluble fraction of sALS compared with controls. In the pellet fraction, PARP-IR was increased by 78% in the sALS sample compared with the control sample. In the soluble fraction, PARP-IR was decreased by 50% in the sALS sample compared with the control sample (Fig. 8C).

DISCUSSION

Recent demonstrations of the presence of markers for oxidative stress in the CNS of sALS patients suggest a putative role for oxidative damage in ALS pathogenesis (2–5, 7, 8, 12–14). Oxidative stress can induce DNA strand breaks, which subsequently triggers the activation of PARP (19–21, 23–25). Alzheimer disease and MPTP-induced Parkinson disease are associated with increased oxidative stress and display increased PARP- and PAR-immunostaining in affected brain tissue (34, 38). Therefore, to determine if PARP expression was also increased in sALS spinal cord tissue, we evaluated the levels of PARP in postmortem tissue of sALS and non-neurological disease control patients. As with Alzheimer and

←

Fig. 4. PARP-IR in control and sALS spinal cord sections. **A–H:** Distribution of PARP-positive profiles from control **(A, C, E, G)** and sALS **(B, D, F, H)** spinal cords. The PARP-IR is nuclear in all sections examined. Peroxidase reaction. Magnification: ×10 in the ventral **(A, B)** and dorsal cord **(C, D)**; ×120 in the lateral column **(E, F)** and in the ventral horn **(G, H)**.

Downloaded from https://academic.oup.com/jnen/article/62/1/88/2917760 by Dokuz Eylul University Library (DEU) user on 02 September 2021

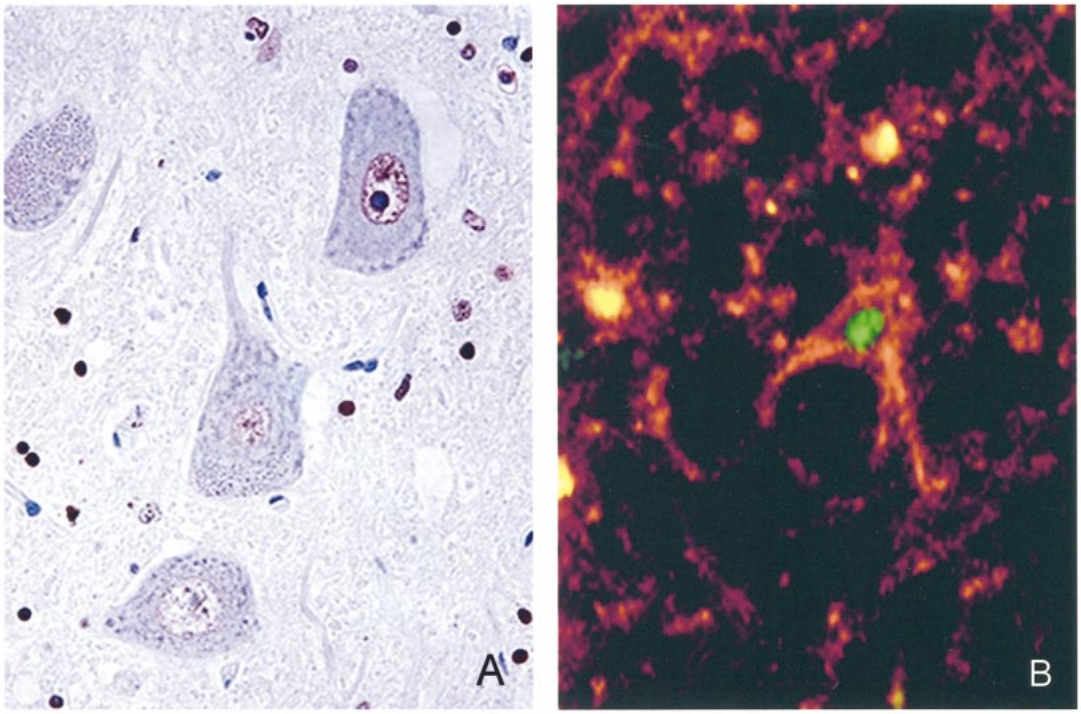

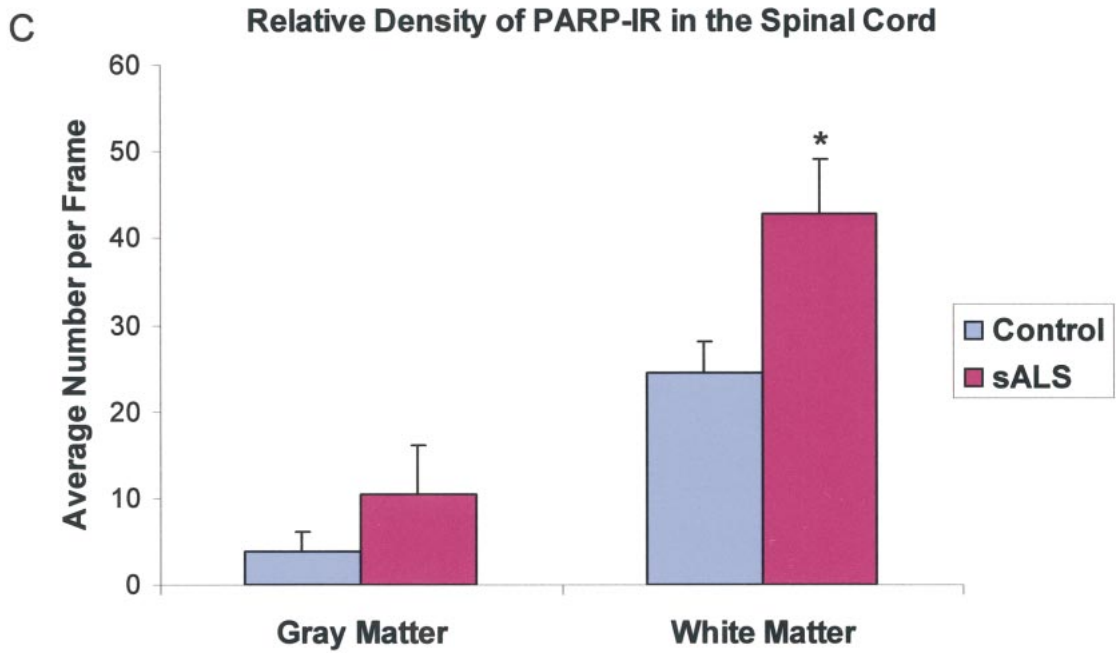

Fig. 5. PARP-IR in neurons and astrocytes in sALS spinal cord tissue. **A:** PARP-positive profiles in the ventral horn from sALS spinal cord tissue. Peroxidase reaction, cresyl violet counterstain. Magnification: ×120. **B:** Astrocytes in the lateral corticospinal tract of the spinal cord from sALS. The green fluorescence indicates PARP-IR in the nuclei, while the red fluorescence corresponds to the GFAP-IR in the cell body and processes. Immunofluorescence. Magnification: ×155. **C:** The graph illustrates that the density of the stained profiles (number of stained nuclei per field) is larger in the sALS spinal cord than in the control tissue, both in the white matter (4,E and 4,F) (1.8Xs; $p = 0.016$) and in the gray matter (4,G and 4,H) (2.7Xs), although not significantly in the later ($p = 0.23$). Data are reported as group means ± SEM.

Downloaded from https://academic.oup.com/jnen/article/62/1/88/2917760 by Dokuz Eylul University Library (DEU) user on 02 September 2021

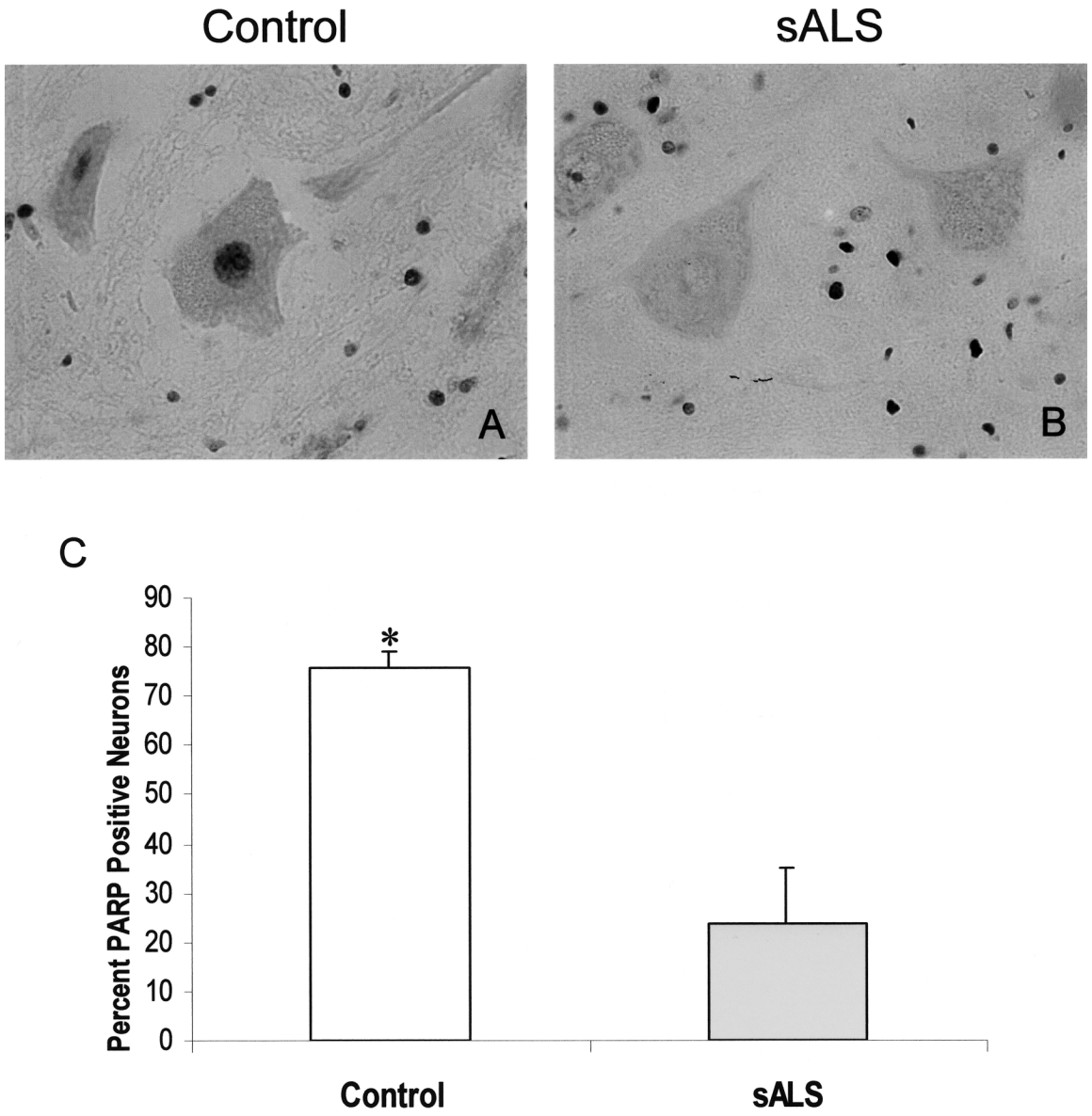

Fig. 6. PARP-IR in motor neurons from control and sALS sections. **A, B:** Representative fields of motor neurons from spinal cords of control **(A)** and sALS patients **(B)** after PARP-immunostaining. The nuclei of the majority of motor neurons in the control tissue proved to be PARP-positive; whereas in the sALS spinal cord, PARP-positive nuclei in motor neurons were rarely encountered. Peroxidase reaction. Magnification: ×240. **C:** The graph represents the mean PARP-positive neurons as a percent of total motor neurons in each field examined ± the SEM. Control sections had significantly more PARP-positive motor neurons as a percentage of motor neurons than the sALS sections ($p < 0.0014$).

MPTP-induced Parkinson diseased tissue, we demonstrated increased PARP-IR in sALS tissue compared with control.

To examine whether pro- or activated caspase 3 expression was altered in sALS compared with control tissues, immunoblot analyses were performed with sALS and control spinal cord samples using 2 different caspase-3 antibodies (CPP32 and CM_1). Procaspase-3 immunoreactivity was readily detected in both sALS and control tissues; however, the immunoreactivity was similar in the 2 groups. No activated caspase-3 was detected in the spinal cord from sALS patients or controls using either antibody; however, the tissues we examined were harvested and frozen with an average delay of approximately 10 h postmortem.

After observing the results of the immunoblot, we anticipated that the increased PARP immunoreactivity would reflect enhanced expression in neurons, perhaps in response to single strand DNA breaks due to increased oxidative stress and/or to increased intracellular Ca^{++}. However, our immunohistochemical studies demonstrated that the 3-fold increase PARP-IR noted in Western blots

Downloaded from https://academic.oup.com/jnen/article/62/1/88/2917760 by Dokuz Eylul University Library (DEU) user on 02 September 2021

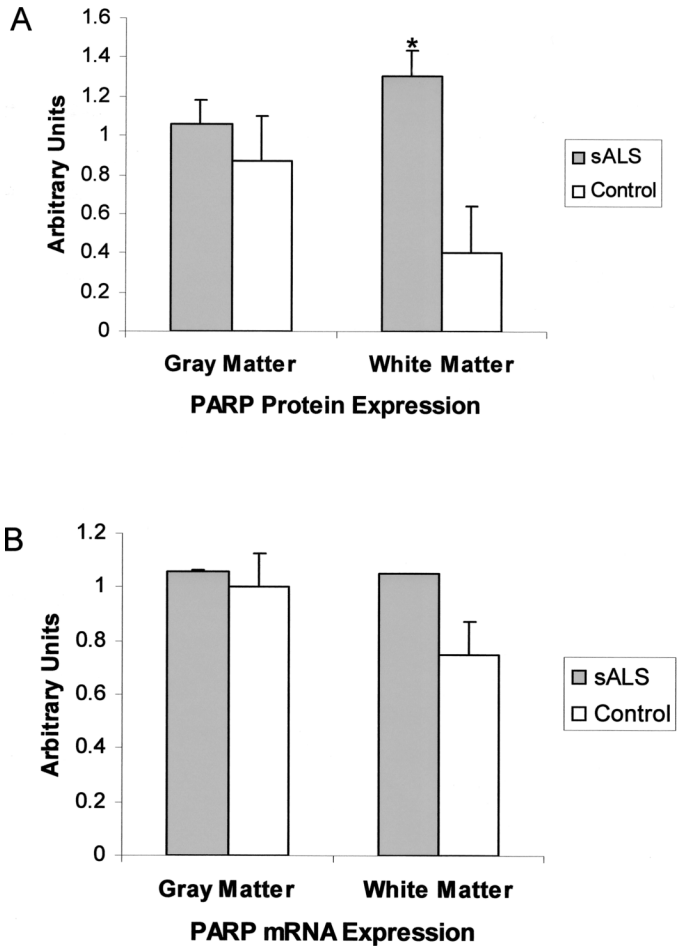

Fig. 7. Protein and mRNA expression in white and gray matter from sALS and control patients. **A, B**: White matter was dissected away from the gray matter of sALS and control samples. Part of the tissue was used to evaluate PARP protein expression **(A)** and the remaining tissue was used to examine PARP mRNA expression **(B).** In the sALS samples, PARP-IR was not increased in the gray matter ($p = 0.53$) but was significantly increased in the white matter ($p = 0.04$) compared with control samples. PARP mRNA in the sALS samples was not increased in the gray matter ($p = 0.62$) or in the white matter ($p = 0.32$) compared with control samples.

from sALS spinal cord specimens was a reflection of glial rather than neuronal PARP-IR. The morphology of cells with increased PARP-IR suggested that astrocytes were the predominant cell type stained, and double antibody staining for PARP and GFAP confirmed that astrocytes were the most common cell type expressing PARP-IR. This staining pattern in sALS tissue is different from the pattern of PARP immunostaining seen in Lewy body disease, where neurons contained the most intense PARP-IR (51) and different from the PARP and PAR immunostaining seen in tissues from Alzheimer or MPTP-induced Parkinson patients, where neurons were the most common cell type containing PAR-IR and astrocytes contained the least (34, 38). Although only PAR-IR was examined in the MPTP-induced Parkinson tissues, it is a reflection of PARP activity.

Although PARP-IR was increased in sALS spinal cord tissue, the mRNA for PARP was not increased significantly in the same specimens. If the increase PARP protein were due to astrogliosis, the increased astrocytic cell division would result in an increase in PARP mRNA; however, that was not the case. Several reasons why the PARP protein would be elevated, without an increased mRNA level, are an increased translation rate, increased protein stability, or slowed degradation, none of which can be directly examined in postmortem tissue. To determine if an altered distribution of PARP could explain the increased PARP-IR, we examined the distribution of PARP-IR in soluble and pellet fractions. We noted that the pellet PARP-IR was largely increased in sALS compared with control samples, while the soluble PARP-IR was decreased in sALS compared with control samples. The enhanced binding of PARP to the pellet fraction in sALS tissues (perhaps to chromatin, nuclear cytoskeleton, and/or nuclear membranes) could potentially stabilize the protein and/or protect it from degradation, and could explain the increased PARP-IR in the absence of a significant increase in PARP mRNA. PARP is known to interact with chromatin, centrosomes, transcription factors, cdk2, and p53 (52–54) and recently with F-actin and rhoA, a

→

Fig. 8. PARP expression in the soluble and pellet fractions of spinal cord homogenates from sALS and control patients. **A:** Homogenized tissue samples from sALS and control patients were divided into 2 aliquots. The first aliquot from each group was separated into the soluble (S) and pellet (P) fractions and 150 mg of protein of each were loaded into a gel for Western analysis. One hundred fifty μg of protein from the second unseparated aliquot was also loaded (H). Blots were probed with anti-PARP monoclonal antibody (7D3-6). Standard molecular weight markers in kilodaltons are indicated. **B:** Homogenized tissue samples from sALS and control patients were divided into 2 aliquots, each containing 250 μg protein. The first aliquot was separated into the soluble (S) and pellet (P) fractions and loaded in their entirety. The second 250-μg aliquot was also loaded in its entirety (H). Blots were probed with anti-PARP monoclonal antibody (7D3-6). ECL signals were compared after 30 s and 10 min of exposure times. In the 30-s ECL exposure, PARP-IR of the whole homogenate (similar to that shown in Fig. 1) and the pellet fraction were already visible (upper panels), however, detection of soluble fractions required 10 min of exposure time (middle panels). The same membranes were stripped and reprobed with anti-actin antibody for normalization. Standard molecular weight markers in kilodaltons are indicated. The results from **(A)** and **(B)** suggest that PARP may be binding to membranes and/or chromatin, which could perhaps stabilize the PARP protein. **C:** Percent of PARP-IR is expressed for homogenate, supernatant, and pellet.

Downloaded from https://academic.oup.com/jnen/article/62/1/88/2917760 by Dokuz Eylul University Library (DEU) user on 02 September 2021

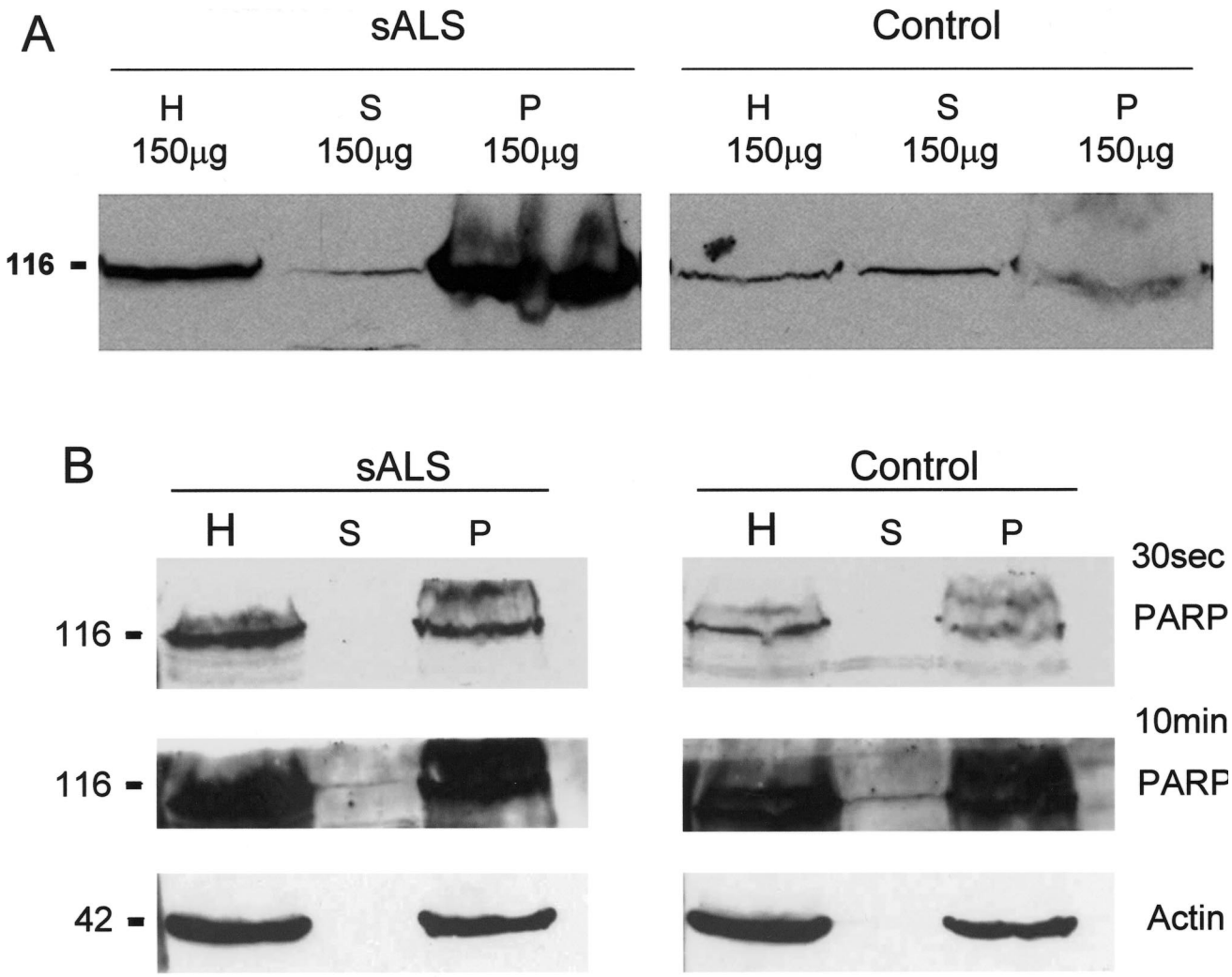

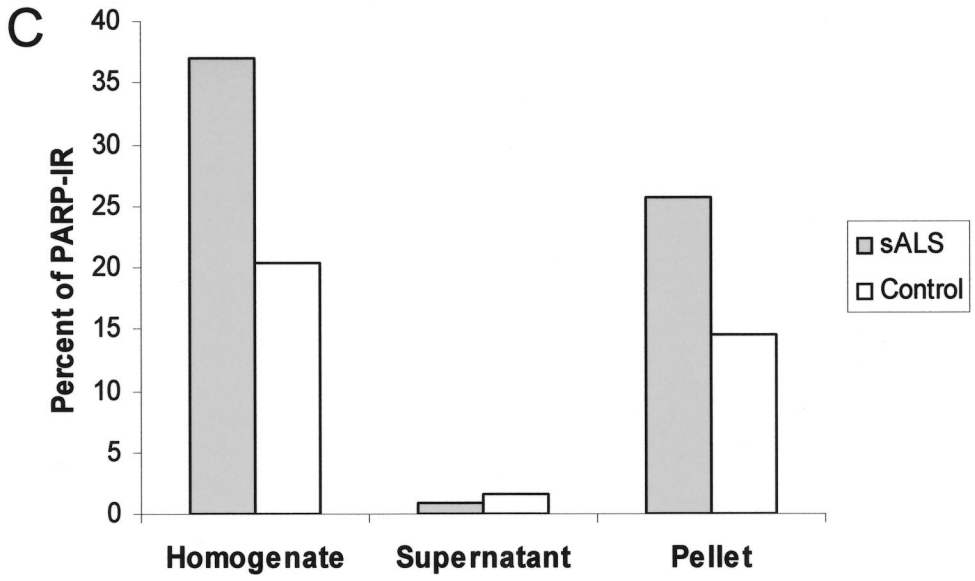

Downloaded from https://academic.oup.com/jnen/article/62/1/88/2917760 by Dokuz Eylul University Library (DEU) user on 02 September 2021

membrane binding protein (55), any of which could stabilize PARP. Interestingly, Figure 5a shows enhanced PARP staining of the nuclear membrane and other structures in the nucleus. PARP is probably not binding to the protein aggregates seen in the cytoplasm and not the nucleus of ALS tissues (12, 56–69), unless the PARP immunoreactivity in the aggregate is somehow blocked.

Given that neurons were the most common cell type expressing PARP and PAR-IR in Alzheimer (38) and MPTP-induced Parkinson (34) disease tissue, diseases also associated with increased oxidative stress; the decreased PARP-IR staining of large motor neurons in sALS was unexpected. It is possible that spinal motor neurons respond differently to oxidative stress than brain neurons affected in Alzheimer disease and Parkinson disease. Since we were examining postmortem tissue, it is also possible that PARP is increased in motor neurons early in the disease and decreases in terminal stages of sALS. It has been shown that measures of oxidative stress in the animal model for ALS (mSOD1) are increasing as the disease progresses (15, 70, 71). Perhaps PARP expression increases until excessive PARP activation leads to energy depletion, resulting in a protective suppression of PARP expression. Such a protective response might suppress the expression of PARP to conserve energy in nonproliferating cells. Surviving motor neurons in sALS would then be able to give priority to essential ATP-dependent processes. However, we cannot rule out the possibility that PARP expression was never increased in sALS motor neurons. PARP has been reported to mediate NMDA but not non-NMDA excitotoxicity (46), and the major glutamate receptor in motor neurons is the AMPA/Kainate receptor (72–78). However, some large motor neurons expressing increased PARP-IR were present in the sALS tissues, arguing against neuronal PARP never increasing in motor neurons. Studies in the sALS transgenic animal model (mSOD1) may help clarify the expression levels of PARP as the disease progresses and the mechanisms modulating its expression in motor neurons.

Recently, treatment with a PARP inhibitor beginning on day 28 resulted in a nonsignificant ($p = 0.08$) trend toward increased survival of the mSOD1 mouse (4% increase) (79). On the basis of our findings, one could speculate that if PARP expression was downregulated in motor neurons at 30 to 40 days, no additional benefit would be obtained by the continued administration of PARP inhibitors. However, no benefit would occur if PARP expression were never increased in sALS motor neurons. Further studies are essential to define the significance and time frame of the enhanced PARP-IR in glia, as well as how and why PARP-IR may be downregulated in sALS motor neurons.

PARP can be activated by single or double-strand breaks in DNA (80–82), and the present demonstration of increased expression of this DNA repair enzyme in sALS is in agreement with previous reports of oxidative damage to DNA and other macromolecules in sALS (2–14). Furthermore, the increased PARP-IR in glia in sALS is in accord with other demonstrations of alterations of astrocytes in response to oxidative stress in ALS (8, 14, 15, 17, 18) and in other systems (83–85), including alterations in the glutamate transporter, GLT-1 or EAAT2 (8, 18, 86–89). Excessive oxidative stress can result in increased PARP expression in astrocytes and can ultimately result in energy depletion and death of the astrocyte (25, 29, 32, 90, 91). Since astroglia may represent an important source of antioxidant protection (92–95) and neurotrophic factors (93–96), the increased PARP-IR in glia may indicate a somewhat compromised ability to mediate critical neuroprotective functions. At the very least, these data demonstrate that the pathological process is not limited to neurons but involves glia in a significant way.

REFERENCES

1. Haverkamp LJ, Appel V, Appel SH. Natural history of amyotrophic lateral sclerosis in a database population. Validation of a scoring system and a model for survival prediction. Brain 1995;118:707–19
2. Bowling AC, Schulz JB, Brown RH Jr,Beal MF. Superoxide dismutase activity, oxidative damage, and mitochondrial energy metabolism in familial and sporadic amyotrophic lateral sclerosis. J Neurochem 1993;61:2322–25
3. Shaw PJ, Ince PG, Falkous G, Mantle D. Oxidative damage to protein in sporadic motor neuron disease spinal cord. Ann Neurol 1995;38:691–95
4. Abe K, Pan LH, Watanabe M, Kato T, Itoyama Y. Induction of nitrotyrosine-like immunoreactivity in the lower motor neuron of amyotrophic lateral sclerosis. Neurosci Lett 1995;199:152–54
5. Beal MF, Ferrante RJ, Browne SE, Matthews RT, Kowall NW, Brown RH Jr. Increased 3-nitrotyrosine in both sporadic and familial amyotrophic lateral sclerosis. Ann Neurol 1997;42:644–54
6. Tohgi H, Abe T, Yamazaki K, Murata T, Ishizaki E, Isobe C. Remarkable increase in cerebrospinal fluid 3-nitrotyrosine in patients with sporadic amyotrophic lateral sclerosis. Ann Neurol 1999;46:129–31
7. Ferrante RJ, Browne SE, Shinobu LA, et al. Evidence of increased oxidative damage in both sporadic and familial amyotrophic lateral sclerosis. J Neurochem 1997;69:2064–74
8. Pedersen WA, Fu W, Keller JN, et al. Protein modification by the lipid peroxidation product 4-hydroxynonenal in the spinal cords of amyotrophic lateral sclerosis patients. Ann Neurol 1998;44:819–24
9. Smith RG, Henry YK, Mattson MP, Appel SH. Presence of 4-hydroxynonenal in cerebrospinal fluid of patients with sporadic amyotrophic lateral sclerosis. Ann Neurol 1998;44:696–99
10. Fitzmaurice PS, Shaw IC, Kleiner HE, et al. Evidence for DNA damage in amyotrophic lateral sclerosis. Muscle Nerve 1996;19:797–98
11. Bogdanov M, Brown RH, Matson W, et al. Increased oxidative damage to DNA in ALS patients. Free Radic Biol Med 2000;29:652–58
12. Chou SM, Wang HS, Komai K. Colocalization of NOS and SOD1 in neurofilament accumulation within motor neurons of amyotrophic lateral sclerosis: An immunohistochemical study. J Chem Neuroanat 1996;10:249–58
13. Chou SM, Han CY, Wang HS, Vlassara H, Bucala R. A receptor for advanced glycosylation endproducts (AGEs) is colocalized with neurofilament-bound AGEs and SOD1 in motoneurons of ALS: Immunohistochemical study. J Neurol Sci 1999;169:87–92

Downloaded from https://academic.oup.com/jnen/article/62/1/88/2917760 by Dokuz Eylul University Library (DEU) user on 02 September 2021

14. Shibata N, Nagai R, Uchida K, et al. Morphological evidence for lipid peroxidation and protein glycoxidation in spinal cords from sporadic amyotrophic lateral sclerosis patients. Brain Res 2001;917: 97–104
15. Sasaki S, Warita H, Abe K, Iwata M. Inducible nitric oxide synthase (iNOS) and nitrotyrosine immunoreactivity in the spinal cords of transgenic mice with a G93A mutant SOD1 gene. J Neuropathol Exp Neurol 2001;60:839–46
16. Sasaki S, Shibata N, Komori T, Iwata M. iNOS and nitrotyrosine immunoreactivity in amyotrophic lateral sclerosis. Neurosci Lett 2000;291:44–48
17. Cha CI, Chung YH, Shin CM, et al. Immunocytochemical study on the distribution of nitrotyrosine in the brain of the transgenic mice expressing a human Cu/Zn SOD mutation. Brain Res 2000; 853:156–61
18. Rothstein JD, Van Kammen M, Levey AI, Martin LJ, Kuncl RW. Selective loss of glial glutamate transporter GLT-1 in amyotrophic lateral sclerosis. Ann Neurol 1995;38:73–84
19. Schraufstatter IU, Hinshaw DB, Hyslop PA, Spragg RG, Cochrane CG. Oxidant injury of cells. DNA strand-breaks activate polyadenosine diphosphate-ribose polymerase and lead to depletion of nicotinamide adenine dinucleotide. J Clin Invest 1986;77:1312–20
20. Zhang J, Dawson VL, Dawson TM, Snyder SH. Nitric oxide activation of poly(ADP-ribose) synthetase in neurotoxicity. Science 1994;263:687–89
21. Virag L, Salzman AL, Szabo C. Poly(ADP-ribose) synthetase activation mediates mitochondrial injury during oxidant-induced cell death. J Immunol 1998;161:3753–59
22. Farkas B, Magyarlaki M, Csete B, et al. Reduction of acute photodamage in skin by topical application of a novel PARP inhibitor. Biochem Pharmacol 2002;63:921–32
23. Cookson MR, Ince PG, Shaw PJ. Peroxynitrite and hydrogen peroxide induced cell death in the NSC34 neuroblastoma x spinal cord cell line: Role of poly (ADP-ribose) polymerase. J Neurochem 1998;70:501–8
24. Karczewski JM, Peters JG, Noordhoek J. Prevention of oxidant-induced cell death in Caco-2 colon carcinoma cells after inhibition of poly(ADP-ribose) polymerase and Ca2+ chelation: Involvement of a common mechanism. Biochem Pharmacol 1999;57:19–26
25. Ying W, Sevigny MB, Chen Y, Swanson RA. Poly(ADP-ribose) glycohydrolase mediates oxidative and excitotoxic neuronal death. Proc Natl Acad Sci U S A 2001;98:12227–32
26. Vispe S, Yung TM, Ritchot J, Serizawa H, Satoh MS. A cellular defense pathway regulating transcription through poly(ADP-ribosyl)ation in response to DNA damage. Proc Natl Acad Sci U S A 2000 Aug 29;97:9886–91
27. Zhang J, Pieper A, Snyder SH. Poly(ADP-ribose) synthetase activation: An early indicator of neurotoxic DNA damage. J Neurochem 1995;65:1411–14
28. Homburg S, Visochek L, Moran N, et al. A fast signal-induced activation of Poly(ADP-ribose) polymerase: A novel downstream target of phospholipase c. J Cell Biol 2000;150:293–307
29. Garthwaite G, Goodwin DA, Batchelor AM, Leeming K, Garthwaite J. Nitric oxide toxicity in CNS white matter: An in vitro study using rat optic nerve. Neuroscience 2002;109:145–55
30. Satoh MS, Lindahl T. Role of poly(ADP-ribose) formation in DNA repair. Nature 1992;356:356–58
31. Ha HC, Snyder SH. Poly(ADP-ribose) polymerase is a mediator of necrotic cell death by ATP depletion. Proc Natl Acad Sci U S A 1999 Nov 23;96:13978–82
32. Schraufstatter IU, Hyslop PA, Hinshaw DB, Spragg RG, Sklar LA, Cochrane CG. Hydrogen peroxide-induced injury of cells and its prevention by inhibitors of poly(ADP-ribose) polymerase. Proc Natl Acad Sci U S A 1986;83:4908–12
33. Wallis RA, Panizzon KL, Henry D, Wasterlain CG. Neuroprotection against nitric oxide injury with inhibitors of ADP-ribosylation. Neuroreport 1993;5:245–48
34. Mandir AS, Przedborski S, Jackson-Lewis V, et al. Poly(ADP-ribose) polymerase activation mediates 1-methyl-4-phenyl-1, 2,3,6-tetrahydropyridine (MPTP)-induced parkinsonism. Proc Natl Acad Sci U S A 1999;96:5774–79
35. Cosi C, Marien M. Implication of poly (ADP-ribose) polymerase (PARP) in neurodegeneration and brain energy metabolism. Decreases in mouse brain NAD+ and ATP caused by MPTP are prevented by the PARP inhibitor benzamide. Ann N Y Acad Sci 1999; 890:227–39
36. Cosi C, Marien M. Decreases in mouse brain NAD+ and ATP induced by 1-methyl-4-phenyl-1, 2,3,6-tetrahydropyridine (MPTP): Prevention by the poly(ADP-ribose) polymerase inhibitor, benzamide. Brain Res 1998;809:58–67
37. Cosi C, Colpaert F, Koek W, Degryse A, Marien M. Poly(ADP-ribose) polymerase inhibitors protect against MPTP-induced depletions of striatal dopamine and cortical noradrenaline in C57B1/6 mice. Brain Res 1996;729:264–69
38. Love S, Barber R, Wilcock GK. Increased poly(ADP-ribosyl)ation of nuclear proteins in Alzheimer's disease. Brain 1999;122:247–53
39. Endres M, Scott G, Namura S, et al. Role of peroxynitrite and neuronal nitric oxide synthase in the activation of poly(ADP-ribose) synthetase in a murine model of cerebral ischemia-reperfusion. Neurosci Lett 1998;248:41–44
40. Endres M, Wang ZQ, Namura S, Waeber C, Moskowitz MA. Ischemic brain injury is mediated by the activation of poly(ADP-ribose) polymerase. J Cereb Blood Flow Metab 1997;17:1143–51
41. Eliasson MJ, Sampei K, Mandir AS, et al. Poly(ADP-ribose) polymerase gene disruption renders mice resistant to cerebral ischemia. Nat Med 1997;3:1089–95
42. Endres M, Scott GS, Salzman AL, Kun E, Moskowitz MA, Szabo C. Protective effects of 5-iodo-6-amino-1,2-benzopyrone, an inhibitor of poly(ADP-ribose) synthetase against peroxynitrite-induced glial damage and stroke development. Eur J Pharmacol 1998;351: 377–82
43. Love S, Barber R, Wilcock GK. Neuronal accumulation of poly(ADP-ribose) after brain ischaemia. Neuropathol Appl Neurobiol 1999;25:98–103
44. Love S, Barber R, Wilcock GK. Apoptosis and expression of DNA repair proteins in ischaemic brain injury in man. Neuroreport 1998; 9:955–59
45. Scott GS, Jakeman LB, Stokes BT, Szabo C. Peroxynitrite production and activation of poly (adenosine diphosphate-ribose) synthetase in spinal cord injury. Ann Neurol 1999;45:120–24
46. Mandir AS, Poitras MF, Berliner AR, et al. NMDA but not non-NMDA excitotoxicity is mediated by Poly(ADP-ribose) polymerase. J Neurosci 2000;20:8005–11
47. Hivert B, Cerruti C, Camu W. Hydrogen peroxide-induced motoneuron apoptosis is prevented by poly ADP ribosyl synthetase inhibitors. Neuroreport 1998;9:1835–38
48. Beer R, Franz G, Srinivasan A, et al. Temporal profile and cellular distribution of activated caspase-3 following experimental traumatic brain injury. J Neurochem 2000;75:1264–73
49. Su JH, Nichol KE, Sitch T, et al. DNA damage and activated caspase-3 expression in neurons and astrocytes: Evidence for apoptosis in frontotemporal dementia. Exp Neurol 2000;163:9–19
50. Draude G, Lorenz RL. TGF-beta1 downregulates CD36 and scavenger receptor A but upregulates LOX-1 in human macrophages. Am J Physiol Heart Circ Physiol 2000;278:H1042–48
51. Love S. Damage to nuclear DNA in Lewy body disease. Neuroreport 2001;12:2725–29
52. Kanai M, Uchida M, Hanai S, Uematsu N, Uchida K, Miwa M. Poly(ADP-ribose) polymerase localizes to the centrosomes and chromosomes. Biochem Biophys Res Commun 2000;278:385–89

Downloaded from https://academic.oup.com/jnen/article/62/1/88/2917760 by Dokuz Eylul University Library (DEU) user on 02 September 2021

53. Santilli G, Cervellera MN, Johnson TK, Lewis RE, Iacobelli S, Sala A. PARP co-activates B-MYB through enhanced phosphorylation at cyclin/cdk2 sites. Oncogene 2001;20:8167–74
54. Tong WM, Cortes U, Wang ZQ. Poly(ADP-ribose) polymerase: A guardian angel protecting the genome and suppressing tumorigenesis. Biochim Biophys Acta 2001;1552:27–37
55. Uchida M, Hanai S, Uematsu N, et al. Overexpression of poly(ADP-ribose) polymerase disrupts organization of cytoskeletal F-actin and tissue polarity in Drosophila. J Biol Chem 2002;277: 6696–6702
56. Nakano I, Hirano A. Atrophic cell processes of large motor neurons in the anterior horn in amyotrophic lateral sclerosis: Observation with silver impregnation method. J Neuropathol Exp Neurol 1987; 46:40–49
57. Shibata N, Hirano A, Kobayashi M, et al. Cu/Zn superoxide dismutase-like immunoreactivity in Lewy body-like inclusions of sporadic amyotrophic lateral sclerosis. Neurosci Lett 1994;179:149–52
58. Shibata N, Hirano A, Kobayashi M, et al. Intense superoxide dismutase-1 immunoreactivity in intracytoplasmic hyaline inclusions of familial amyotrophic lateral sclerosis with posterior column involvement. J Neuropathol Exp Neurol 1996;55:481–90
59. Chou SM, Wang HS, Taniguchi A. Role of SOD-1 and nitric oxide/cyclic GMP cascade on neurofilament aggregation in ALS/MND. J Neurol Sci (Suppl.) 1996;139:16–26
60. Shibata N, Asayama K, Hirano A, Kobayashi M. Immunohistochemical study on superoxide dismutases in spinal cords from autopsied patients with amyotrophic lateral sclerosis. Dev Neurosci 1996;18:492–98
61. Bruijn LI, Becher MW, Lee MK, et al. ALS-linked SOD1 mutant G85R mediates damage to astrocytes and promotes rapidly progressive disease with SOD1-containing inclusions. Neuron 1997; 18:327–38
62. Bruijn LI, Houseweart MK, Kato S, et al. Aggregation and motor neuron toxicity of an ALS-linked SOD1 mutant independent from wild-type SOD1. Science 1998;281:1851–54
63. Ince PG, Tomkins J, Slade JY, Thatcher NM, Shaw PJ. Amyotrophic lateral sclerosis associated with genetic abnormalities in the gene encoding Cu/Zn superoxide dismutase: Molecular pathology of five new cases, and comparison with previous reports and 73 sporadic cases of ALS. J Neuropathol Exp Neurol. 1998;57:895–904
64. Johnston JA, Dalton MJ, Gurney ME, Kopito RR. Formation of high molecular weight complexes of mutant Cu, Zn-superoxide dismutase in a mouse model for familial amyotrophic lateral sclerosis. Proc Natl Acad Sci U S A 2000;97:12571–76
65. Stieber A, Gonatas JO, Gonatas NK. Aggregates of mutant protein appear progressively in dendrites, in periaxonal processes of oligodendrocytes, and in neuronal and astrocytic perikarya of mice expressing the SOD1(G93A) mutation of familial amyotrophic lateral sclerosis. J Neurol Sci 2000;177:114–23
66. Stieber A, Gonatas JO, Gonatas NK. Aggregation of ubiquitin and a mutant ALS-linked SOD1 protein correlate with disease progression and fragmentation of the Golgi apparatus. J Neurol Sci 2000; 173:53–62
67. Watanabe M, Dykes-Hoberg M, Culotta VC, Price DL, Wong PC, Rothstein JD. Histological evidence of protein aggregation in mutant SOD1 transgenic mice and in amyotrophic lateral sclerosis neural tissues. Neurobiol Dis 2001;8:933–41
68. Kato S, Sumi-Akamaru H, Fujimura H, et al. Copper chaperone for superoxide dismutase co-aggregates with superoxide dismutase 1 (SOD1) in neuronal Lewy body-like hyaline inclusions: An immunohistochemical study on familial amyotrophic lateral sclerosis with SOD1 gene mutation. Acta Neuropathol (Berl) 2001;102:233–38
69. Wang J, Xu G, Borchelt DR. High molecular weight complexes of mutant superoxide dismutase 1: Age-dependent and tissue-specific accumulation. Neurobiol Dis 2002;9:139–48
70. Andrus PK, Fleck TJ, Gurney ME, Hall ED. Protein oxidative damage in a transgenic mouse model of familial amyotrophic lateral sclerosis. J Neurochem 1998;71:2041–48
71. Hall ED, Andrus PK, Oostveen JA, Fleck TJ, Gurney ME. Relationship of oxygen radical-induced lipid peroxidative damage to disease onset and progression in a transgenic model of familial ALS. J Neurosci Res 1998;53:66–77
72. Williams TL, Day NC, Ince PG, Kamboj RK, Shaw PJ. Calcium-permeable alpha-amino-3-hydroxy-5-methyl-4-isoxazole propionic acid receptors: A molecular determinant of selective vulnerability in amyotrophic lateral sclerosis. Ann Neurol 1997;42:200–207
73. Vandenberghe W, Ihle EC, Patneau DK, Robberecht W, Brorson JR. AMPA receptor current density, not desensitization, predicts selective motoneuron vulnerability. J Neurosci 2000;20:7158–66
74. Pizzi M, Benarese M, Boroni F, Goffi F, Valerio A, Spano PF. Neuroprotection by metabotropic glutamate receptor agonists on kainate-induced degeneration of motor neurons in spinal cord slices from adult rat. Neuropharmacology 2000;39:903–10
75. Greig A, Donevan SD, Mujtaba TJ, Parks TN, Rao MS. Characterization of the AMPA-activated receptors present on motoneurons. J Neurochem 2000;74:179–91
76. Roy J, Minotti S, Dong L, Figlewicz DA, Durham HD. Glutamate potentiates the toxicity of mutant Cu/Zn-superoxide dismutase in motor neurons by postsynaptic calcium-dependent mechanisms. J Neurosci 1998;18:9673–84
77. Bar-Peled O, O'Brien RJ, Morrison JH, Rothstein JD. Cultured motor neurons possess calcium-permeable AMPA/kainate receptors. Neuroreport 1999;10:855–59
78. Metzger F, Wiese S, Sendtner M. Effect of glutamate on dendritic growth in embryonic rat motoneurons. J Neurosci 1998;18:1735–42
79. Andreassen OA, Dedeoglu A, Friedlich A, et al. Effects of an inhibitor of poly(ADP-ribose) polymerase, desmethylselegiline, trientine, and lipoic acid in transgenic ALS mice. Exp Neurol 2001;168: 419–24
80. Berger NA. Poly(ADP-ribose) in the cellular response to DNA damage. Radiat Res 1985;101:4–15
81. Carson DA, Seto S, Wasson DB, Carrera CJ. DNA strand breaks, NAD metabolism, and programmed cell death. Exp Cell Res 1986; 164:273–81
82. de Murcia G, Menissier de Murcia J. Poly(ADP-ribose) polymerase: A molecular nick-sensor. Trends Biochem Sci 1994;19:172–76
83. Brand A, Leibfritz D, Richter-Landsberg C. Oxidative stress-induced metabolic alterations in rat brain astrocytes studied by multinuclear NMR spectroscopy. J Neurosci Res 1999;58:576–85
84. Servitja JM, Masgrau R, Pardo R, Sarri E, Picatoste F. Effects of oxidative stress on phospholipid signaling in rat cultured astrocytes and brain slices. J Neurochem 2000;75:788–94
85. Cassina P, Peluffo H, Pehar M, et al. Peroxynitrite triggers a phenotypic transformation in spinal cord astrocytes that induces motor neuron apoptosis. J Neurosci Res 2002;67:21–29
86. Trotti D, Rolfs A, Danbolt NC, Brown RH Jr,Hediger MA. SOD1 mutants linked to amyotrophic lateral sclerosis selectively inactivate a glial glutamate transporter. Nat Neurosci 1999;2:427–33
87. Volterra A, Trotti D, Tromba C, Floridi S, Racagni G. Glutamate uptake inhibition by oxygen free radicals in rat cortical astrocytes. J Neurosci 1994;14:2924–32
88. Trotti D, Rossi D, Gjesdal O, Levy LM, Racagni G, Danbolt NC, Volterra A. Peroxynitrite inhibits glutamate transporter subtypes. J Biol Chem 1996;271:5976–79
89. Miralles VJ, Martinez-Lopez I, Zaragoza R, et al. Na+ dependent glutamate transporters (EAAT1, EAAT2, and EAAT3) in primary astrocyte cultures: Effect of oxidative stress. Brain Res 2001;922: 21–29
90. Ying W, Swanson RA. The poly(ADP-ribose) glycohydrolase inhibitor gallotannin blocks oxidative astrocyte death. Neuroreport 2000;11:1385–88

Downloaded from https://academic.oup.com/jnen/article/62/1/88/2917760 by Dokuz Eylul University Library (DEU) user on 02 September 2021

91. Robb SJ, Robb-Gaspers LD, Scaduto RC Jr,Thomas AP, Connor JR. Influence of calcium and iron on cell death and mitochondrial function in oxidatively stressed astrocytes. J Neurosci Res 1999;55: 674–86
92. Tanaka J, Toku K, Zhang B, Ishihara K, Sakanaka M, Maeda N. Astrocytes prevent neuronal death induced by reactive oxygen and nitrogen species. Glia 1999;28:85–96
93. Desagher S, Glowinski J, Premont J. Astrocytes protect neurons from hydrogen peroxide toxicity. J Neurosci 1996;16:2553–62
94. Lindsay RM. Adult rat brain astrocytes support survival of both NGF-dependent and NGF-insensitive neurones. Nature 1979;282: 80–82
95. Hori O, Matsumoto M, Kuwabara K, et al. Exposure of astrocytes to hypoxia/reoxygenation enhances expression of glucose-regulated protein 78 facilitating astrocyte release of the neuroprotective cytokine interleukin 6. J Neurochem 1996;66:973–79
96. Thoenen H, Hughes RA, Sendtner M. Trophic support of motoneurons: Physiological, pathophysiological, and therapeutic implications. Exp Neurol 1993;124:47–55

Received May 6, 2002
Revision received August 15, 2002 and October 3, 2002
Accepted October 14, 2002

Downloaded from https://academic.oup.com/jnen/article/62/1/88/2917760 by Dokuz Eylul University Library (DEU) user on 02 September 2021